Attosecond Time Delay in Bound–Bound Transitions Probed by Fano Resonances

Zhigang Zheng[1,2], Li Wang[1,2,3], Di Wang[1,2], Mingyue Wang[1,2], Fan Xiao[1,2], Jing Zhao[1,2,3], Xiaowei Wang[1,2,3*], and Zengxiu Zhao[1,2,3*]

[1]*Department of Physics, National University of Defense Technology, Changsha 410073, China*
[2]*Hunan Key Laboratory of Extreme Matter and Applications, National University of Defense Technology, Changsha 410073, China*
[3]*Hunan Research Center of the Basic Discipline for Physical States, National University of Defense Technology, Changsha 410073, China*

(Received 11 June 2025; accepted manuscript online 1 August 2025)

This letter presents a method for probing the attosecond time delay between two radiatively resonant transitions from Fano structures, which arise from interference between the extreme ultraviolet free induction decay (XFID) emission and high-order harmonics. The ellipticity dependence of the Ne^+ XFID yield confirms that the ionic excited-state populations originate from inelastic recollision between tunneling electrons and parent ions. Subsequent extraction of relative phases from Fano structures enables the determination of the time delay (~ 22 as) between the two decay pathways. This work provides an experimental approach to probe the attosecond time delay between different XFID channels and contributes to a deeper understanding of the tunneling-plus-rescattering model in strong laser fields.

DOI: 10.1088/0256-307X/42/9/090302 CSTR: 32039.14.0256-307X.42.9.090302

Strong-field ionization, excitation, and radiation are crucial physical phenomena arising from the interaction of strong laser fields with matter. Some semiclassical models and theoretical frameworks have been developed during several decades to clarify ultrafast electron dynamics in strong laser fields, such as the tunneling-plus-rescattering model.[1–3] Moreover, precise monitoring of ionized electrons and emitted photons provides essential diagnostics for tracking the evolution of the quantum state.[4–6] Throughout these studies, the attosecond time delays between different physical processes have always been a fundamental parameter for establishing unified spatiotemporal descriptions of ultrafast strong field dynamics.

Recent advances in attosecond science and technology have enabled precise measurements of time delays in tunneling ionization and photoemission, which are fundamental issues in strong-field physics. While certain studies suggest that strong field tunneling occurs quasi-instantaneously with negligible time delays,[7–13] others report measurable non-zero time delays supported by experimental and theoretical results.[14–20] Furthermore, some theoretical and experimental studies consistently indicate that the time delay in photoemission is on the order of tens of attoseconds.[21–25] Although debate continues regarding these temporal characteristics, the time-resolved dynamics of post-ionization electronic processes remain comparatively unexplored. Recent breakthroughs by Wang *et al.*[26] revealed attosecond-scale time differences between resonant transition channels induced by Raman processes in ions, demonstrating delays correlated with spin–orbit coupling strengths. Notably, research on the temporal characteristics of the extreme ultraviolet (XUV) free induction decay (XFID) process, a critical pathway for encoding multielectron correlations, remains scarce.

In this Letter, attosecond time delay between distinct XFID channels is resolved through Fano structures, which arise from interference between neon ionic XFID radiation and high-order harmonics (HH). In the experiment, few-cycle laser pulses ionize neon atoms and populate the excited ionic state, $2s2p^6$ ($^2S_{1/2}$), from the ground state, $2s^22p^5$ ($^2P^o_{1/2}$) and $2s^22p^5$ ($^2P^o_{3/2}$). The ellipticity dependence of the Ne^+ XUV spectra validates that the excitation is achieved through the tunneling electron rescattering process. Subsequently, the excited neon ions emit XUV photons via the FID process. The interference between the XFID radiation and the HH results in a Fano structure in the spectrum, from which the XFID and HH components, along with their relative phases, can be extracted. Finally, the attosecond time delay between different XFID channels is derived from the phase differences. This work not only provides direct experimental validation for the rescattering excitation mechanism, but also reveals time delays between different XFID channels, thereby advancing the mechanistic understanding of radiation dynamics in strong laser fields.

In the experiment, the laser system (Femtopower Pro HE) delivered pulses with 4.2 mJ energy, 25 fs duration, 800 nm central wavelength at 1 kHz repetition rate.

*Corresponding authors. Email: xiaowei.wang@nudt.edu.cn; zhaozengxiu@nudt.edu.cn
© 2025 Chinese Physical Society and IOP Publishing Ltd. All rights, including for text and data mining, AI training, and similar technologies, are reserved.

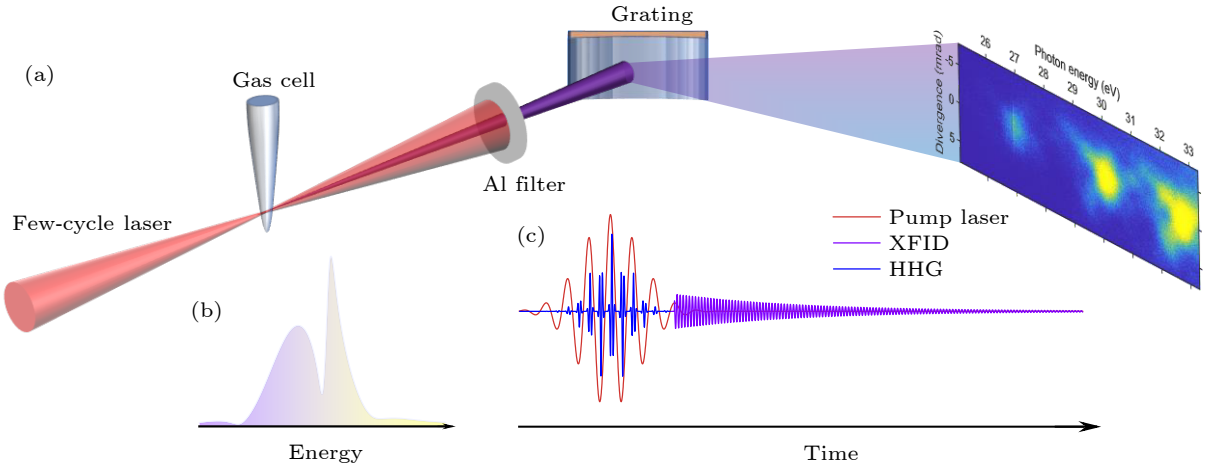

Fig. 1. (a) Schematic of the experimental setup. The spectrum in the right panel shows experimental measurements. (b) Characteristic Fano structure in the spectrum arising from interference between HH and XFID. (c) The electric field of pump laser and corresponding temporal evolution of HH generation (HHG) and XFID emission. (b) and (c) schematically illustrate the Fano resonance structure in the frequency domain and its corresponding time-domain waveform, respectively.

Table 1. A summary of Ne^+ transition parameters.

Lower level			Upper level			Photon energy	RI	A_{ki}
Conf.	Term	J	Conf.	Term	J	(eV)		(10^9 s^{-1})
$2s^22p^5$	$^2P^o$	3/2	$2s2p^6$	^2S	1/2	26.9105	2000	5.54
			$2s^22p^4(^3P)3s$	^4P	5/2	27.1688	240	–
			$2s^22p^4(^3P)3s$	^4P	3/2	27.2329	400	–
			$2s^22p^4(^3P)3s$	^4P	1/2	27.2700	300	–
$2s^22p^5$	$^2P^o$	1/2	$2s2p^6$	^2S	1/2	26.8137	1000	2.70
			$2s^22p^4(^3P)3s$	^4P	3/2	27.1362	180	–
			$2s^22p^4(^3P)3s$	^4P	1/2	27.1732	22	–

Few-cycle pulses (8 fs duration, 720 nm central wavelength, 1 mJ energy) were generated through spectral broadening in a hollow-core fiber and compression via chirped mirror pairs. These pulses were focused by a 500-mm-focal-length lens onto neon atoms within a gas cell featuring a 1 mm inner diameter. Crucially, the gas pressure was optimized at 90 mbar through systematic scans where harmonic yield demonstrated quadratic pressure dependence, so that the experiments were conducted within the phase-matching regime that minimizes propagation-induced spectral distortions. At the focus, the peak intensity reached 2 PW/cm^2. The generated XUV radiation passed through a 200-nm aluminum foil filter and was dispersed by a grazing-incidence grating spectrometer, with spectra recorded using an XUV camera (Dhyana XF400BSI-PS), as schematized in Fig. 1(a).

The harmonic spectrum near 27 eV exhibited interference structures upon the Gaussian profile, which were identified as Fano profiles.[27–29] As schematically illustrated in Figs. 1(b) and 1(c), these asymmetric line shapes arise from quantum interference between a discrete transition (Lorentzian-broadened) and a continuum. Figure 1(b) shows the characteristic Fano asymmetry, while Fig. 1(c) demonstrates its temporal origin: the few-cycle pump laser (red curve) drives the HH (blue curve) localized near the field maxima, producing attosecond bursts. Subsequent XFID emission (purple curve) persists for hundreds of femtoseconds to picoseconds after laser extinction.[30] This temporal dichotomy manifests spectrally as interference between the broadband HH (instantaneous Gaussian signal) and narrowband XFID (continuous Lorentzian signal). The resulting Fano structure directly encodes the relative quantum phase between HH and XFID pathways, providing a time-frequency ruler for strong-field dynamics.

According to Refs. [31,32] and NIST databases,[33] there are multiple Ne^+ excited states near 27 eV capable of emitting XFID radiation, which can interfere with HH to form the Fano resonances, as shown in Table 1. The experimentally calibrated Fano peaks at 26.82 eV and 26.93 eV correspond to the $2s2p^6$ ($^2S_{1/2}$) $\rightarrow$ $2s^22p^5$ ($^2P^o_{1/2}$) and $2s2p^6$ ($^2S_{1/2}$) $\rightarrow$ $2s^22p^5$ ($^2P^o_{3/2}$) transitions, respectively. This assignment is confirmed by agreement with relative intensities (RI) and Einstein coefficients (A_{ki}) in Table 1. The slight discrepancies ($\sim$0.02 eV) between calibrated and theoretical transition energies may originate from systematic uncertainties in harmonic peak calibration and Fano profile reconstruction.

The observed XFID radiation confirms the significant population of ionic excited states by the strong laser fields. While atomic Rydberg state excitation in strong laser fields is typically attributed to frustrated tunneling ionization mechanisms,[3] the preparation of ionic

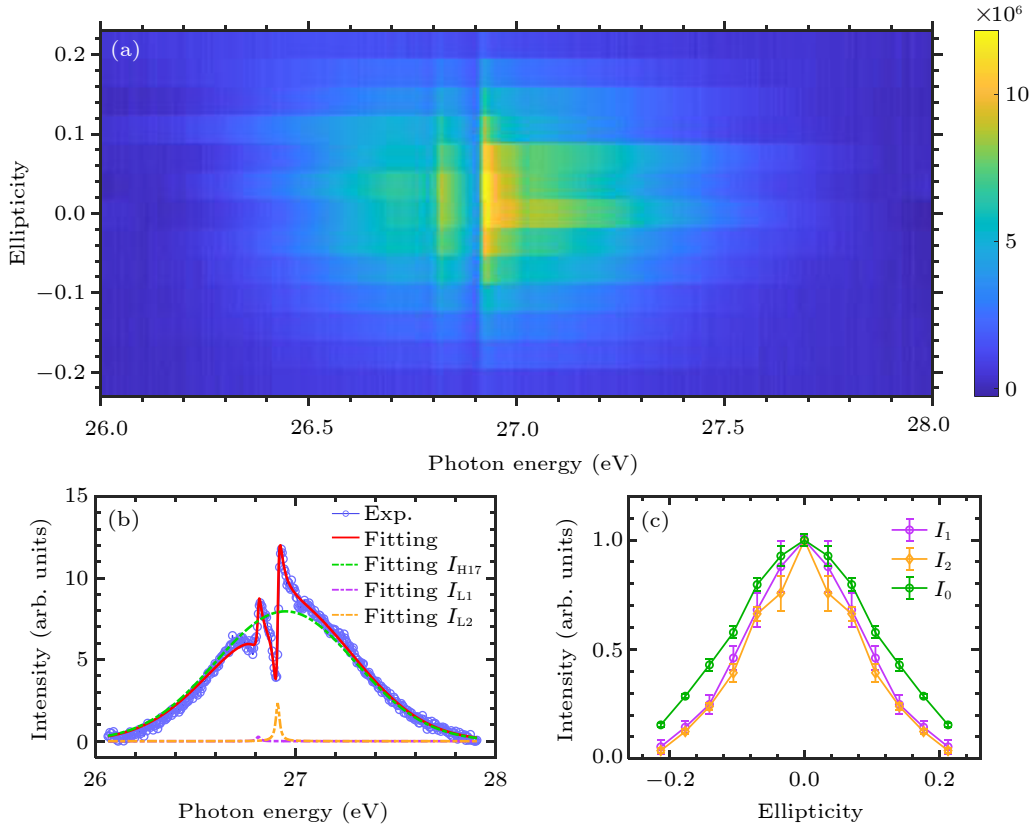

Fig. 2. (a) Averaged Fano-structured spectra (26–28 eV) versus laser ellipticity (ϵ) from quintuplicate measurements. (b) The spectrum and fitting results at $\epsilon = 0$. The blue data corresponds to the experimental measurements, while the red curve represents the global fit. The green dashed is the fitted Gaussian profile of the 17th harmonic (H17, I_{H17}). The purple and yellow dashed are fitted Lorentzian profiles of the two XFIDs, corresponding to the transitions $2s2p^6\ (^2S_{1/2}) \rightarrow 2s^22p^5\ (^2P^o_{1/2})$ (I_{L1}) and $2s2p^6\ (^2S_{1/2}) \rightarrow 2s^22p^5\ (^2P^o_{3/2})$ (I_{L2}), respectively. (c) Ellipticity dependence of normalized peak intensities of H17 (I_0) and XFIDs (I_1, I_2). Error bars denote $\pm 1\sigma$ standard deviation from five measurements.

inner-shell excited states remains less explored. Within the tunneling-plus-rescattering framework, tunneling electrons may transfer energy to the parent ion through inelastic rescattering events during recollision trajectories, thereby exciting the ion to various excited states with finite probability. To validate this mechanism, the ellipticity-dependence XUV spectra were measured, as shown in Fig. 2(a). Each spectrum was fitted using the following formula:

$$I = I_0 \left| e^{-2\ln 2\left(\frac{\omega-\omega_0}{\Delta\omega}\right)^2} + \frac{B_1}{\Gamma_1}\frac{1-i\varepsilon_1}{1+\varepsilon_1^2}e^{i\varphi_1} + \frac{B_2}{\Gamma_2}\frac{1-i\varepsilon_2}{1+\varepsilon_2^2}e^{i\varphi_2}\right|^2, \quad (1)$$

where $\varepsilon_i = 2(\omega - \omega_i)/\Gamma_i$ is the reduced energy, ω_i is the resonant frequency, Γ_i is the linewidth of the i-th XFID, φ_i denotes the relative phase between the H17 and XFID, I_0 and B_i are the corresponding amplitude coefficients, ω_0 is the central frequency of H17, $\Delta\omega$ is the full width of half maximum of H17. Crucially, while Eq. (1) describes ideal coherent interference, the extracted relative phase φ_i remains robust under partial coherence conditions, since the phase information is encoded in spectral asymmetry.

The fitting results (red line) for linearly polarized laser ($\epsilon = 0$) are presented in Fig. 2(b), demonstrating excellent agreement with the experimental spectrum (blue line). The green, purple, and yellow dashed lines represent the fitting spectra of H17, $I_{\mathrm{H17}} = I_0 e^{-4\ln 2\left(\frac{\omega-\omega_0}{\Delta\omega}\right)^2}$ and two XFIDs, $I_i = I_0\left(\frac{B_i}{\Gamma_i}\right)^2 \frac{1}{\varepsilon_i^2+1}$, respectively. Figure 2(c) shows the ellipticity dependence of normalized peak intensities of XFIDs, $I_i = I_0(B_i/\Gamma_i)^2$ $(i = 1, 2)$, and H17, I_0. Strikingly, both $I_i(\epsilon)$ and $I_0(\epsilon)$ exhibit similar trends, unambiguously linking the production of Ne^+ excited states to the same rescattering dynamics that drives HH. Consequently, the population of the Ne^+ excited states corresponds to a different outcome of the tunneling electron rescattering process compared to high-order harmonics generation (HHG). As shown in Fig. 3, the tunneling electrons undergo inelastic collisions with Ne^+ during the rescattering process. While the electrons escape, they simultaneously populate the Ne^+ to the excited states. Finally, the excited Ne^+ emits XUV photons via the FID process.

From the fitting results in Fig. 2(b), the phases φ_i $(i = 1, 2)$ for both Fano structures are extracted, with the ellipticity dependence presented in Fig. 4. Since φ_i represents the relative phase between two XFID signals with

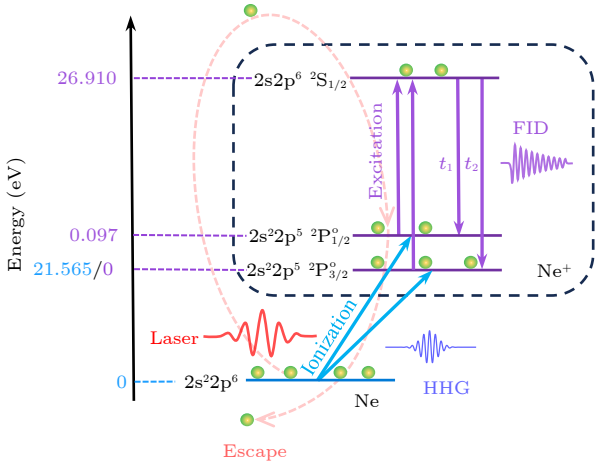

Fig. 3. Energy-level diagram depicting ionization, excitation, and radiation dynamics in strong laser fields. The blue numerical labels correspond to energy levels of the neutral Ne atom, and the purple numerical labels correspond to energy levels of the Ne^+ ion. The energy zero point (0 eV) for the Ne^+ ion levels is set at the ionic ground state. The electron dynamics are described in detail in the text.

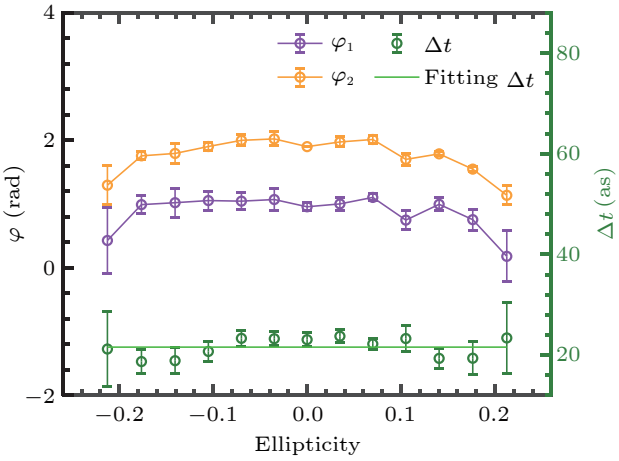

Fig. 4. The dependence of phases and derived time delays Δt on laser ellipticity. Error bars represent the standard deviation of the relative phase obtained from five repeated HH spectral measurements at each ellipticity.

respect to the same order harmonic H17, the phase difference $\Delta\varphi = \varphi_1 - \varphi_2$ reveals the relative phase between the two XFID channels and reflects temporal asynchrony in their radiative decay pathways. As shown in Fig. 3, tunnel ionization prepares Ne^+ in a superposition of spin–orbit states, $J = 1/2$ and $3/2$, which are subsequently excited to the common state $2s2p^6$ ($^2S_{1/2}$) via inelastic collisions. The subsequent XFID process involves the ionic excited state decaying back to two states with different transition probabilities, emitting XUV photons with different energies. Crucially, since the excited state $2s2p^6$ ($^2S_{1/2}$) is uniquely determined, the prior population excitation process and the subsequent transition radiation process can be considered independent of each other. As a result, the derived $\Delta\varphi$ is exclusively sensitive to differences in the two radiative decay pathways. Based on the fitting results, the time delay between the transitions, $2s2p^6$ ($^2S_{1/2}$) $\rightarrow$ $2s^22p^5$ ($^2P^o_{3/2}$) and $2s2p^6$ ($^2S_{1/2}$) $\rightarrow$ $2s^22p^5$ ($^2P^o_{1/2}$), is calculated to be $\Delta t \simeq 23 \pm 1.4$ as while $\epsilon = 0$. Remarkably, the delay Δt almost remains constant across varying laser ellipticities, as shown by the flat trend in Fig. 4. The constant value of the green fitting line is approximately 22 as. This invariance suggests that the temporal offset originates from quantum mechanical phase accumulation during the decay process itself, rather than ellipticity-dependent excitation dynamics. This is because variations in laser ellipticity change the trajectories of tunneled electrons within the laser field, which affects both HHG and inelastic collisional excitation processes.

Due to the intrinsic attosecond chirp in HHG, the phase variation introduced by the harmonic energy difference between two transition pathways should also be taken into account. Coulomb-corrected classical trajectory simulations were performed within the over-the-barrier (OTB) framework [34] to quantify the energy-dependent time delay using experimental parameters. The results show that the excursion time differences of short- and long-trajectory electrons corresponding to the two transition energies are 0.5 as and 0.3 as, respectively, which are much smaller than the experimentally derived delay 22 as. This indicates that the HHG chirp contributes negligibly to the measured time delay, instead highlighting spin–orbit-induced wavepacket bifurcation during XFID emission as the dominant mechanism.

In summary, few-cycle laser pulses are employed to ionize neon atoms and excite the Ne^+ $2s2p^6$ ($^2S_{1/2}$) state via tunneling ionization followed by inelastic recollision processes. The resulting XFID spectra interfere with the 17th harmonic, forming distinct Fano structures. By fitting the Fano structures, the dependence of intensity and phase on ellipticity validates the recollision-driven excitation mechanism. Crucially, phase-resolved quantum interference reveals an attosecond time delay of $\sim$22 as between the $2s2p^6$ ($^2S_{1/2}$) $\rightarrow$ $2s^22p^5$ ($^2P^o_{3/2}$) and $2s^22p^5$ ($^2P^o_{1/2}$) transition pathways. This work establishes a general experimental framework for resolving transition-specific attosecond time delays in atomic and ionic systems, while advancing the understanding of coherent XFID dynamics in strong laser fields.

Acknowledgements. This work was supported by the National Natural Science Foundation of China (Grant Nos. 12234020, 12474281, 12450403, and 12274461), and the Science and Technology Innovation Program of Hunan Province (Grant No. 2022RC1193).

References

[1] Corkum P B 1993 *Phys. Rev. Lett.* **71** 1994
[2] Lewenstein M, Balcou P, Ivanov M Y, L'Huillier A, and Corkum P B 1994 *Phys. Rev. A* **49** 2117
[3] Nubbemeyer T, Gorling K, Saenz A, Eichmann U, and Sandner W 2008 *Phys. Rev. Lett.* **101** 233001
[4] Krausz F and Ivanov M 2009 *Rev. Mod. Phys.* **81** 163
[5] Ossiander M, Siegrist F, Shirvanyan V, Pazourek R, Sommer A, Latka T, Guggenmos A, Nagele S, Feist J, Burgdörfer J, Kienberger R, and Schultze M 2017 *Nat. Phys.* **13** 280

[6] Sabbar M, Timmers H, Chen Y, Pymer A K, Loh Z, Sayres S, Pabst S, Santra R, and Leone S R 2017 *Nat. Phys.* **13** 472

[7] Eckle P, Pfei er A N, Cirelli C, Staudte A, Dörner R, Muller H G, Büttiker M, and Keller U 2008 *Science* **322** 1525

[8] Pfei er A N, Cirelli C, Smolarski M, Dimitrovski D, and Abusamha M, Madsen L B, and Keller U 2012 *Nat. Phys.* **8** 76

[9] Torlina L, Morales F, Kaushal J, Ivanov I, Kheifets A, Zielinski A, Scrinzi A, Muller H G, Sukiasyan S, Ivanov M, and Smirnova O 2015 *Nat. Phys.* **11** 503

[10] Ni H C, Saalmann U, and Rost J 2016 *Phys. Rev. Lett.* **117** 023002

[11] Klaiber M, Hatsagortsyan K Z, and Keitel C H 2018 *Phys. Rev. Lett.* **120** 013201

[12] Quan W, Serov V V, Wei M Z, Zhao M, Zhou Y, Wang Y L, Lai X Y, Kheifets A S, and Liu X J 2019 *Phys. Rev. Lett.* **123** 223204

[13] Sainadh U S, Xu H, Wang X S, Atia-tul-noor A, Wallace W C, Douguet N, Bray A, Ivanov I, Bartschat K, Kheifets A, Sang R T, and Litvinyuk I V 2019 *Nature* **568** 75

[14] Teeny N, Yakaboylu E, Bauke H, and Keitel C H 2016 *Phys. Rev. Lett.* **116** 063003

[15] Zimmermann T, Mishra S, Doran B R, Gordon D F, and Landsman A S 2016 *Phys. Rev. Lett.* **116** 233603

[16] Camus N, Yakaboylu E, Fechner L, Klaiber M, Laux M, Mi Y H, Hatsagortsyan K Z, Pfeifer T, Keitel C H, and Moshammer R 2017 *Phys. Rev. Lett.* **119** 023201

[17] Ramos R, Spierings D, Racicot I, and Steinberg A M 2020 *Nature* **583** 529

[18] JiangWC, Zhong M C, Fang Y K, Donsa S, Březinová I, Peng L Y, and Burgdörfer J 2024 *Phys. Rev. Lett.* **133** 163201

[19] Xie W H, Li Z C, Li M, Liu Y P, Liu Y, Cao C P, Guo K Y, Liu K L, Zhou Y M, and Lu P X 2024 *Phys. Rev. Lett.* **133** 183201

[20] Shi H Y and Thumm U 2025 *Phys. Rev. A* **111** 013119

[21] Schultze M, Fieß; M, Karpowicz N, Gagnon J, Korbman M, Hofstetter M, Neppl S, Cavalieri A L, Komninos Y, Mercouris Th, Nicolaides C A, Pazourek R, Nagele S, Feist J, Burgdörfer J, Azzeer A M, Ernstorfer R, Kienberger R, Kleineberg U, Goulielmakis E, Krausz F, and Yakovlev V S 2010 *Science* **328** 1658

[22] Klünder K, Dahlström J M, Gisselbrecht M, Fordell T, Swoboda M, Guénot D, Johnsson P, Caillat J, Mauritsson J, Maquet A, Taïeb R, and L'Huillier A 2011 *Phys. Rev. Lett.* **106** 143002

[23] González-Collado C M, Cattaneo L, Plésiat E, Omiste J J, Vos J, González-Vázquez J, Decleva P, Keller U, Palacios A, and Martín F 2024 *Phys. Rev. Res.* **6** 033342

[24] Potamianos D, Schnitzenbaumer M, Lemell C, Scigalla P, Libisch F, Schock-schmidtke E, Haimerl M, Schröder C, Schäer M, Küchle J T, Riemensberger J, Eberle K, Cui Y, Kleineberg U, Burgdörfer J, Barth J V, Feulner P, Allegretti F, and Kienberger R 2024 *Sci. Adv.* **10** eado0073

[25] Biswas S, Trabattoni A, Rupp P, Magrakvelidze M, Madjet M E, De giovannini U, Castrovilli M C, Galli M, Liu Q, and Månsson E P, Schötz J, Wanie V, Wnuk P, Colaizzi L, Mocci D, Reduzzi M, Lucchini M, Nisoli M, Rubio A, Chakraborty H S, Kling M F, and Calegari F 2025 *Sci. Adv.* **11** eads0494

[26] Wang L, Bai G R, Wang X W, Zhao J, Gao C, Wang J C, Xiao F, Tao W K, Song P, Qiu Q Y, Liu J L, and Zhao Z X 2024 *Nat. Commun.* **15** 2705

[27] Fano U 1961 *Phys. Rev.* **124** 1866

[28] Zhao Z X and Lin C D 2005 *Phys. Rev. A* **71** 060702

[29] Ott C, Kaldun A, Raith P, Meyer K, Laux M, Evers J, Keitel C H, Greene C H, and Pfeifer T 2013 *Science* **340** 716

[30] Beaulieu S, Bloch E, Barreau L, Comby A, Descamps D, Géneaux R, Légaré F, Petit S, and Mairesse Y 2017 *Phys. Rev. A* **95** 041401

[31] Persson W 1971 *Phys. Scr.* **3** 133

[32] Baig M A and Connerade J P 1984 *J. Phys. B: Atom. Mol. Phys.* **17** 1785

[33] Kramida A, Ralchenko Y, Reader J, and NIST ASD Team 2024 *NIST Atomic Spectra Database* (version 5.12)

[34] Hostetter J A, Tate J L, Schafer K J, and Gaarde M B 2010 *Phys. Rev. A* **82** 023401